



Heriot-Watt University
Research Gateway

The role of laser pulse overlap in ultrafast thin film structuring applications

Citation for published version:

Geremia, R, Karnakis, D & Hand, DP 2018, 'The role of laser pulse overlap in ultrafast thin film structuring applications', *Applied Physics A: Materials Science and Processing*, vol. 124, no. 9, 641.
<https://doi.org/10.1007/s00339-018-2045-z>

Digital Object Identifier (DOI):

[10.1007/s00339-018-2045-z](https://doi.org/10.1007/s00339-018-2045-z)

Link:

[Link to publication record in Heriot-Watt Research Portal](#)

Document Version:

Publisher's PDF, also known as Version of record

Published In:

Applied Physics A: Materials Science and Processing

General rights

Copyright for the publications made accessible via Heriot-Watt Research Portal is retained by the author(s) and / or other copyright owners and it is a condition of accessing these publications that users recognise and abide by the legal requirements associated with these rights.

Take down policy

Heriot-Watt University has made every reasonable effort to ensure that the content in Heriot-Watt Research Portal complies with UK legislation. If you believe that the public display of this file breaches copyright please contact open.access@hw.ac.uk providing details, and we will remove access to the work immediately and investigate your claim.



The role of laser pulse overlap in ultrafast thin film structuring applications

R. Geremia^{1,2} · D. Karnakis¹ · D. P. Hand²

Received: 1 November 2017 / Accepted: 12 August 2018 / Published online: 24 August 2018
© The Author(s) 2018

Abstract

In this work, we demonstrate the importance of laser pulse overlap in controlling the ablation process of a thin film just above the single pulse material ablation threshold. A 532 nm, 15 ps ultrafast diode pump solid-state (DPSS) laser has been employed to pattern a gold alloy source–drain layer during the production of organic thin film transistor (OTFT) for flexible display applications. Maintaining the laser fluence constantly above and in proximity of the ablation threshold value, different process windows are identified by varying the pulse overlap. With less than four overlapping pulses per area, a debris-free removal process is achieved with almost no edge delamination. By increasing the number of pulses per area up to 20, edge delamination progressively grows stronger and eventually ablation terminates altogether. If the pulse overlap increases further, ablation starts again but with more evidence for thermal, cumulative irradiation effects. This behavior can be attributed to the progressive transition from initially a photomechanical stress-assisted ablation process, dominant at low pulse overlap to increasingly a more thermally driven removal process, at higher pulse overlaps.

1 Introduction

Ultrafast DPSS lasers (ps and fs) present great potential for material functionalization when three-dimensional high precision and accuracy processing is needed. Ultrashort pulses can in fact decouple the rapid laser absorption-induced electronic excitation in a material from removal due to slower thermal effects [1, 2]. Under specific conditions, ablation can be also assisted by laser-induced photomechanical stress [3]. In such a regime, ablation usually takes place at low temperature and material removal is not only energetically more efficient, compared to evaporative ablation, but also any collateral damage inflicted to the material is greatly reduced [4]. Such “cold” ablation regime makes ultrafast lasers an ideal tool for selective thin film patterning where material removal needs to be well controlled to typically few tens of nanometres only [5]. Photomechanically assisted ablation, in combination with ultrafast lasers, has been successfully employed for the production of photovoltaic solar cells [6],

OLEDs [7] and OTFTs for flexible displays [8] as a mask-free and fully digital alternative to photolithography for low volume production. Recently [9], we observed that fine tuning of the laser pulse overlap close to the ablation threshold can produce counterintuitive results. When photomechanical stress-assisted ablation applies, strong delamination or even ablation termination was observed by increasing the pulse overlap. Such effects must be taken into account in an industrial production environment because they can greatly influence the usual tradeoff between process speed and quality.

2 Experimental setup

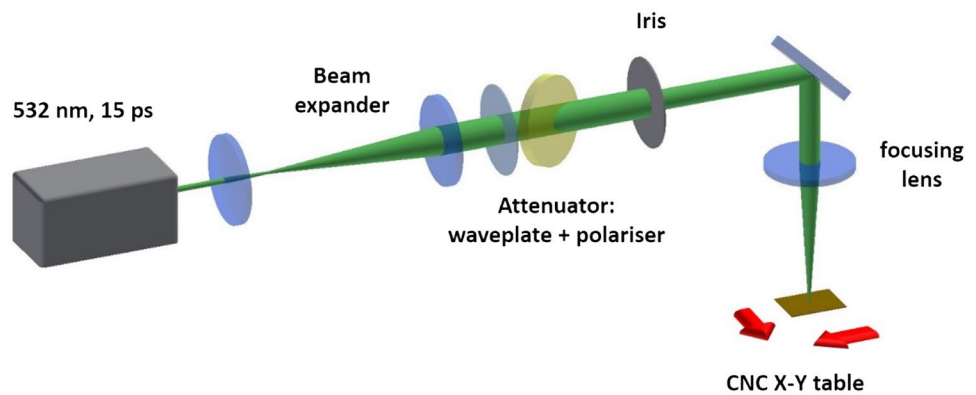
The experimental setup consists of an Oxford Lasers J-Series micromachining system as shown schematically in Fig. 1. The laser source is a Coherent Talisker Ultra, and the 532 nm second-harmonic emitting pulses of nominally less than 15 ps (FWHM) and maximum energy of 22 μJ at 200 kHz have been used with nominal $M^2 < 1.1$. The laser power was measured after the final focusing lens on the workpiece. The Gaussian laser beam was measured to have a diameter of 5.4 mm (at $1/e^2$), and the beam wings were spatially cleaned using a 5.7 mm diameter aperture. The CNC translation table carrying the workpiece consists of an X-Y linear motor axis pair and a motorized vertical Z

✉ R. Geremia
riccardo.geremia@oxfordlasers.com

¹ Oxford Lasers Ltd, Unit 8 Moorbrook Park,
Didcot OX11 7HP, UK

² School of Engineering and Physical Science, Heriot-Watt
University, Edinburgh EH14 4AS, UK

Fig. 1 Sketch of the experimental setup



axis. A 60 mm focal length f-theta lens mounted on the Z axis underneath a galvanometer scanner was used to focus this beam onto the sample. Since the aperture is almost the same size as the beam diameter, mild beam truncation is assumed and the laser spot at the lens focal plane is taken to be diffraction limited, to a diameter of $7.6 \mu\text{m}$ at $1/e^2$. The workpiece is an OTFT multilayer stack of different materials where the top two layers, as encountered by the laser, are 80 nm thick gold alloy thin films over a $5 \mu\text{m}$ thick polymeric planarization layer, transparent at 532 nm. Its mechanical strength is provided by a glass substrate at the bottom of the stack. Sample analysis was performed using a Nikon ECLIPSE LV100 optical microscope and a Zygo Nexview white light interferometer with nominal vertical measurement repeatability of 0.1 nm.

3 Results and discussion

The role of spatial laser pulse overlap was studied by scribing straight lines and analyzing a matrix of incident laser fluence F versus pulse overlap. We define the spatial laser pulse overlap O as the dimensionless number of incident laser pulses per illuminated area, i.e.,

$$O = \frac{w \cdot RR}{s}, \quad (1)$$

where w is the theoretical spot diameter (in mm) on the workpiece estimated at $1/e^2$ of maximum fluence, RR is the laser pulse repetition rate in Hz, and s is the scan speed in mm/s. The single pulse ablation threshold (average) fluence F_{th} for the gold layer was measured to be $F_{th} = 110 \pm 10 \text{ mJ/cm}^2$ (Fig. 2) using the D squared method [10]. Then several sets of test straight channels were patterned on the sample, each on a fresh area. Each set of channels was machined at fixed average fluence. The fluence was progressively increased from 0.8 to 6 times the ablation threshold fluence F_{th} , i.e., in the range 90–660 mJ/cm^2 . Figure 3 shows the most relevant cases, where F is equal to 150 ± 10 and

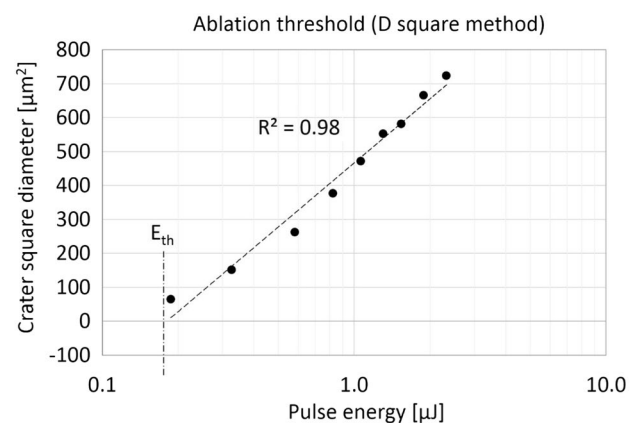


Fig. 2 Ablation threshold determination according to [10]. The energy per pulse is progressively reduced until no crater is left onto the thin film layer. By fitting the craters, squared diameter for each energy point is possible to estimate the minimum energy value needed to mark the material by a single pulse

$200 \pm 10 \text{ mJ/cm}^2$. Every set contains channels machined at different laser pulse overlaps between 0.9 and 34.7 pulses/area. The laser pulse overlap was varied by adjusting the scan speed, while keeping the laser pulse repetition rate constant at 1 kHz. The results appear as mostly a debris-free ablation, with clean and well defined edges when O is kept below 4. In the pulse overlap range $4 < O < 20$, strong delamination arises when $F = 2F_{th}$ and edges present evidence of melting and/or strong plastic deformation. Within this overlap range strong evidence of substrate damage are not visible under both optical microscope and SEM. If, for the same overlap range, the fluence is reduced to $1.5F_{th}$, laser ablation terminates and no material removal takes place with the only exception of the first few pulses of the channel. In fact, at the beginning of each channel, the layer is always ablated for every explored values of overlap and fluence. But if ablation is terminated at any point along the scanning direction, this regime can continue up to the very last pulse of the channel (Fig. 4). By further increasing the laser

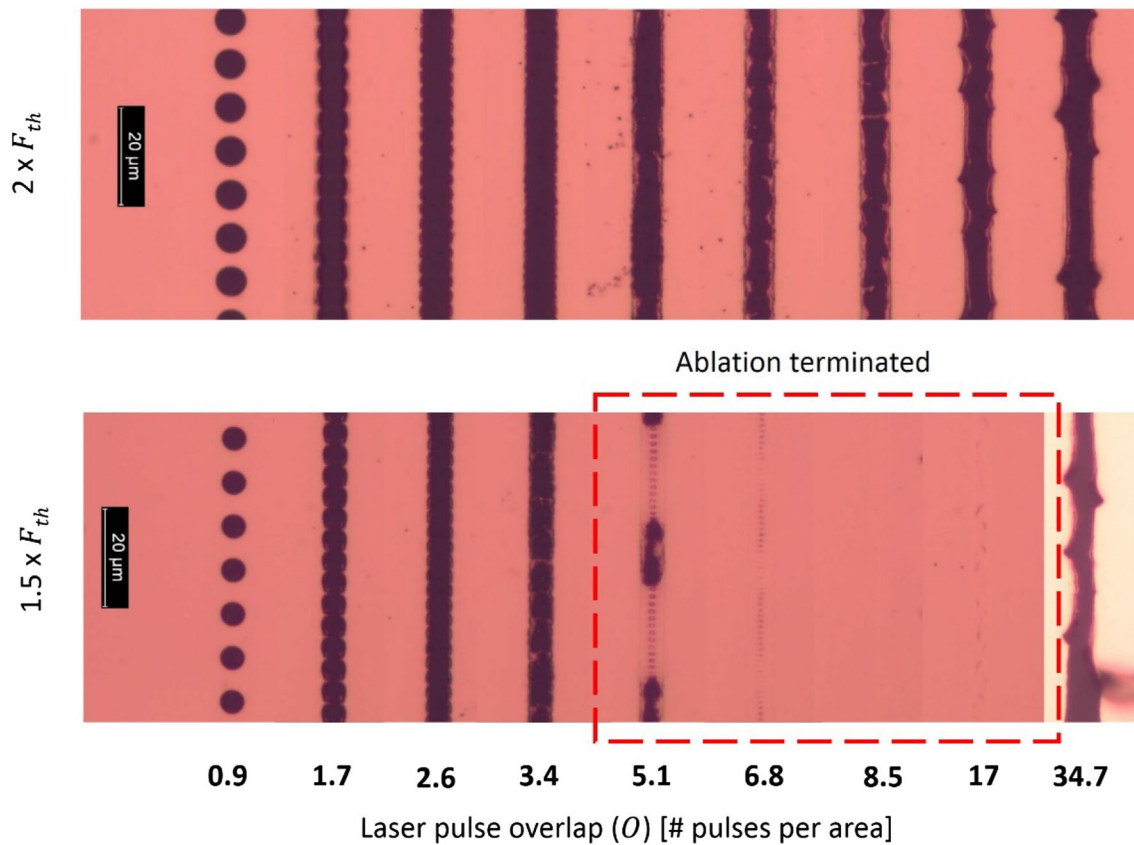


Fig. 3 Matrix of fluence VS laser pulse overlap. The red box highlights the region whereby increasing the overlap, ablation is terminated

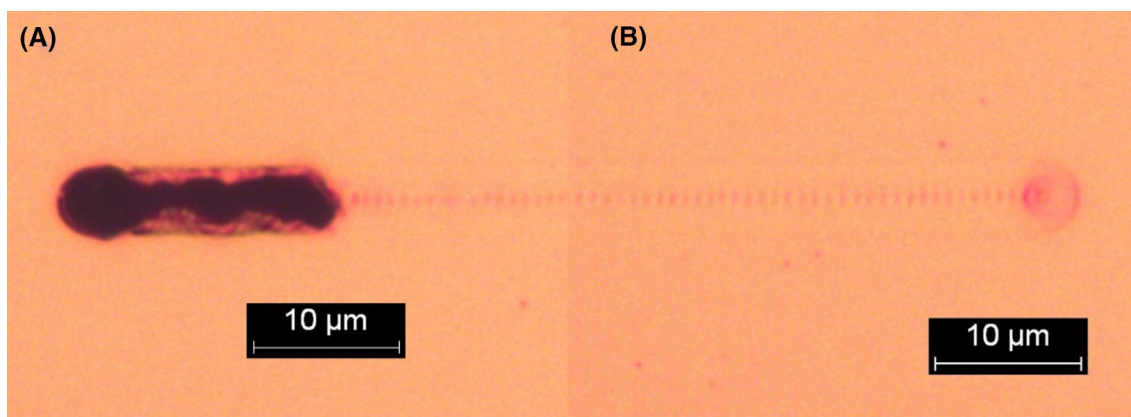


Fig. 4 Start (a) and end (b) of a laser patterned channel on gold layer written at 150 mJ/cm^2 and overlap equal to 8.5

pulse overlap beyond $O > 20$ at this fluence level, ablation starts again and more evident thermal cumulative effects are visible on the edges of the ablated channels as well on the substrate with respect to the lower overlap regions for any $F > F_{th}$. The range of laser pulse overlap, where strong delamination and/or ablation termination is visible, gets larger the closer the fluence is to the F_{th} value. There is no abrupt transition between these two described regimes.

To understand the ablation termination mechanism with increasing overlap, the single pulse case is first discussed. The gold alloy layer normal incidence reflectivity R at 532 nm has been measured by ellipsometry as 69%, with an absorption coefficient μ_a of $5.03 \times 10^5 \text{ cm}^{-1}$ @ 532 nm (real and complex refractive indices, $n = 0.5441$ and $k = 2.1404$). The exact thermal and mechanical properties of the layer are not known and hence those of pure

gold are assumed for the following study, if not otherwise specified.

The energy required to melt and vaporize the irradiated volume ($7.6 \mu\text{m}$ spot size \times 80 nm film thickness) is estimated at $1.2 \times 10^{-7} \text{ J}$, taking bulk gold density $\rho = 19.3 \text{ g/cm}^3$, heat of fusion 12 kJ/mol , heat of vaporization 342 kJ/mol , and atomic mass unit of 197. Assuming no reflectivity changes during the pulse absorption, the energy deposited into the film for a single pulse at threshold is about $1.5 \times 10^{-8} \text{ J}$, lower than that required to melt and vaporize the material. This implies that the temperature rise experienced by the layer on single pulse laser irradiation at F_{th} is insufficient to cause melting. The SEM microscopy images in Fig. 5 support the result of the energy balance showing single pulse craters at fluence F near F_{th} with homogeneous plastic deformation all around the rim but no melting on the edges of the ablated zone nor scattered debris or molten droplets as typically observed in metal ablation. It is, therefore, reasonable to assume that the ablation mechanism is most likely driven by a photomechanical effect [3] and the material is removed mostly in the solid phase. This ablation regime, usually referred as spallation, is typically achieved when both thermal and stress confinement occurs in the heated volume, i.e., when the laser pulse duration τ_p is much shorter than both the characteristic thermal τ_{th} and acoustic τ_{ac} material relaxation times, defined as:

$$\tau_{\text{th}} = \frac{d^2}{4D} \quad (2)$$

$$\tau_{\text{ac}} = \frac{d}{v_s}, \quad (3)$$

where d is the smallest characteristic dimension of the heated volume (either layer thickness, optical penetration,

or heat diffusion depths), D is the thermal diffusivity, and v_s is the speed of sound in gold. In such a case, maximum light absorption takes place in the film; minimal thermal conduction losses and subsequent rapid heating produces very high transient thermoelastic stress that can exceed the film fracture limit before any thermal expansion allows for stress relaxation. Considering d to be equal to the film thickness in this case, bulk gold diffusivity $1.27 \times 10^{-4} \text{ m}^2/\text{s}$, and speed of sound of 2030 m/s , we estimate $\tau_{\text{ac}} = 39 \text{ ps}$ and $\tau_{\text{th}} = 13 \text{ ps}$ which means $\tau_{\text{ac}} \approx \tau_{\text{th}} \approx \tau_p$. Here, because the laser pulse duration is of the same order of magnitude as the characteristic relaxation times, a less efficient conversion of the deposited laser pulse energy into thermoelastic stress is expected as opposed to the clearly defined spallation region where a much shorter pulse $\tau_p \ll \tau_{\text{th}} \wedge \tau_{\text{ac}}$ is used [4]. In fact spallation has been achieved for much longer pulses than the relaxation times during thin film patterning even in the ns regime [11–13]. Longer pulse-driven spallation is mainly possible thanks to the interfaces between layers with different mechanical and thermal properties, acting as additional thermal and stress confining barriers with respect to the case of purely bulk materials. In the work reported here, it is assumed that the lower thermal conductivity of the polymeric planarization substrate compared to the top metallic layer, coupled with the higher Poisson ratio of gold in comparison with polymers, has resulted in the significant increase in efficiency of the spallation process [3, 11].

Given the assumption of removal by spallation a tentative discussion can be developed. The different phases of spallation have been extensively studied both experimentally and through simulations by several groups [3–5, 14–17]. When the laser pulse hits the material surface, part of the energy is lost by reflection. The fraction of energy absorbed by the material is $E_{\text{abs}} = FA(1 - R)$, where F is the average absorbed laser fluence and A is the theoretical laser spot area on the workpiece. Through the light absorption, the irradiated region experiences a rapid, nearly isochoric, temperature rise that leads to compressive stress in the heated volume. Part of E_{abs} is consequently stored as potential energy U within the irradiated volume. U represents the maximum amount of energy that can be coupled into mechanical stresses. When the pulse absorption is concluded the pressure is released by a rapid expansion of the irradiated volume. Such expansion is constrained by both the surrounding gold material at the edges of the irradiated spot and the underlying substrate, but not by the free interface with air. As a result of these boundary conditions a net force is generated, acting on the irradiated volume, accelerating it normal to the surface and away from the substrate. This motion produces a tensile stress at the interface between the film and the substrate. If this tensile stress overcomes both the film yield strength Y and the adhesion force to the polymer substrate, the film fractures and is ejected with kinetic energy K . The

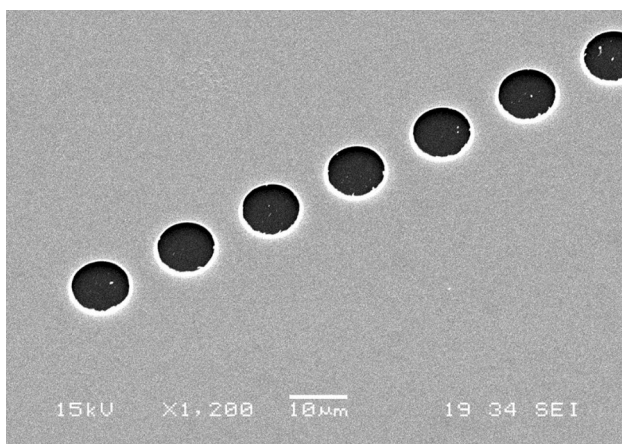


Fig. 5 SEM image of series of single pulse ablated craters in 80 nm thick gold just above the ablation threshold (532 nm , 15 ps , $F = 110 \text{ mJ/cm}^2$)

remaining energy Q that is not coupled into mechanical stress is wasted as heat. As a result E_{abs} can be written as follows:

$$E_{\text{abs}} = U + Q = E_{\text{ad}} + E_{\text{ten}} + K + Q, \tag{4}$$

where E_{ad} is the required energy to overcome the adhesion to the substrate and E_{ten} is the energy needed to overcome the tensile strength of the film. E_{ad} is generally much lower than E_{ten} [11]. Experimentally it is observed how, below F_{th} , a blister is formed over the irradiated area. Such evidence of delaminated but not ablated material below threshold reinforces the assumption that $E_{\text{ad}} \ll E_{\text{ten}}$. In addition, below threshold there is no mass removal which means that, for any $F < F_{\text{th}}$, $K \approx 0$. As a result, for $F = F_{\text{th}}$, we expect $K \ll E_{\text{ten}}$ as well as E_{ad} [12]. The energy balance is therefore reduced to a first approximation, for $F = F_{\text{th}}$, to

$$E_{\text{abs}} \approx U + Q \approx E_{\text{ten}} + Q, \tag{5}$$

where we suppose that the great majority of potential energy storage is spent to fracture the film. The releasing of the potential energy U under the form of rapid expansion and the consequent tensile stress generation can give rise to the propagation of a rarefaction wave [13]. This wave propagates away from the free interface, where the temperature reaches its maximum, toward the substrate. Once the wave is reflected at the interface between the gold layer and the substrate, sufficient tensile stress to brake and eject the film is generated. Therefore, the efficiency of the spallation process is directly dependent on the coupling efficiency of the absorbed energy E_{abs} into the rarefaction wave. The fraction of E_{abs} stored as U is defined by [3]

$$\frac{U}{E_{\text{abs}}} = \frac{1}{4B} \Gamma^2 \mu_a \frac{E_{\text{abs}}}{A}, \tag{6}$$

where B is taken as the gold bulk modulus (180 GPa), Γ is the Grüneisen parameter chosen equal to 3 for all temperatures below the melting point [14]. Substituting all above values, a conversion efficiency of 21% is calculated. As previously discussed, the non-ideal condition of working with $\tau_{\text{ac}} \approx \tau_p$ further decreases the available energy for tensile stress according to a corrective factor $\alpha = (1 - e^{-t})/t$ where $t = \tau_p/\tau_{\text{ac}}$ [4]. For our pulse duration α is 83%. Finally, the mechanical properties of the material need to be considered. Only a fraction of the stored energy will radiate under the form of rarefaction wave. The remaining energy will be retained as quasi-static thermoelastic strain energy and wasted as heat. If the penetration depth is small with respect to the laser spot, as is the case here, so that the rarefaction wave can be considered plane, the fraction f_r of potential energy effectively radiated is [3]

$$f_r = \frac{1 + \nu}{3(1 - \nu)}. \tag{7}$$

With ν being the gold Poisson Ration (0.44) $f_r = 86\%$. Adding together all these efficiency loss contributions, i.e., total energy absorbed, pulse duration corrective factor, and material properties, the energy coupled in the rarefaction wave is only 15% of the total absorbed energy E_{abs} , which in our case is only 2.2nJ. According to (5) this value must be now compared with E_{ten} .

To evaluate E_{ten} the minimum temperature rise ΔT required to generate gold yield strength Y must be estimated. For a disk clipped at the edges, the thermal stress S within the disk resulting from this temperature rise is [15]

$$S = \frac{\beta E_y \Delta T}{2(1 - \nu)}. \tag{8}$$

With β being the linear expansion coefficient ($1.4 \times 10^{-5} \text{ K}^{-1}$) and E_y Young's modulus for gold, which can vary from 30 to 120 GPa depending on crystal orientation [16] and film thickness [17]. The yield stress required to break the material can also vary with respect to film thickness, temperature and crystallographic orientation [18, 19] from 50 MPa [16] up to 260 MPa [20]. Imposing $S = Y$ and considering the mentioned minimum and maximum values from the literature for the parameters in (8), the temperature rise ΔT must range from 33 to 700 K. If our alloy behaves like pure gold, temperature variations within this range are not enough to rise the layer temperature above the gold melting point at 1060 °C starting from room temperature. E_{ten} can now be considered equal to the energy needed to rise the temperature of a mass m by ΔT . Assuming uniform heating and the specific heat of bulk gold $c = 128 \text{ J/(kg K)}$ applicable to our sub- μm thick layer, using $E_{\text{ten}} = mc\Delta T$ gives a value between 0.3 and 6.3 nJ. Remarkably, the above estimated potential energy of 2.2 nJ is within the calculated range and certainly of the same order of magnitude. A more accurate analysis would require knowledge of the exact thermal and mechanical properties of the gold alloy layer material which are unknown. Also, working with $\tau_{\text{ac}} \approx \tau_{\text{th}} \approx \tau_p$ implies that photomechanical effects and film thermal equilibrium occur in a time frame close to the laser pulse duration. We are, therefore, ignoring that thermomechanical properties could change with temperature within the pulse duration.

Following the previous analysis, the dominant contribution to the overall photomechanical removal efficiency is given by (6) and is linearly dependent on the absorbed energy. Since the planarization substrate is transparent at 532 nm it is unlikely that any residual potential energy is stored in the substrate assuming no conduction losses from above within the metal layer ablation timeframe. If only gold can contribute to potential energy storage, the removal efficiency is inversely proportional to the gold area illuminated by the laser pulse on the workpiece and

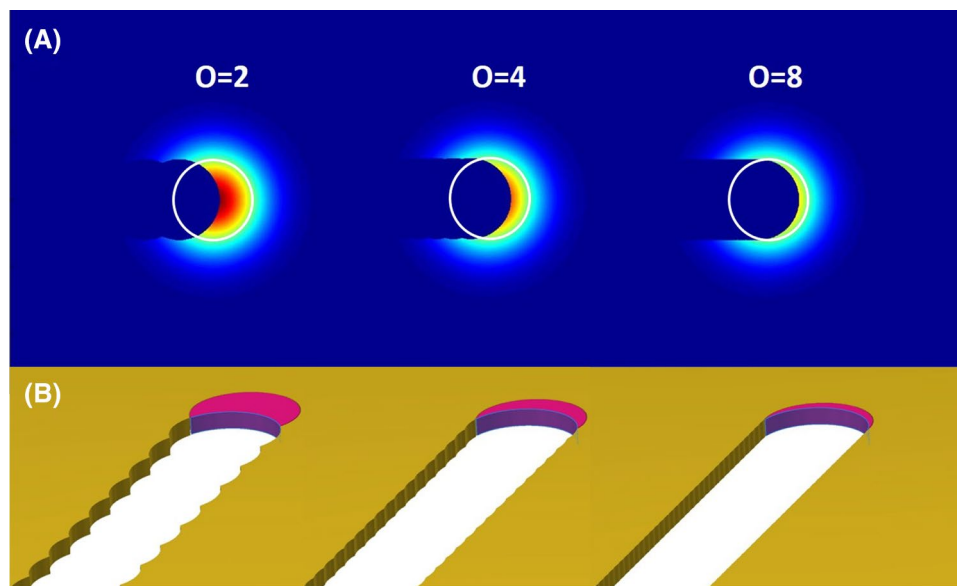


Fig. 6 **a** Graphic representation of the intensity profile seen by the thin film, at the arrival of the front pulse, for different overlaps. Beam dimension at $1/e^2$ and crater dimension simulate the case presented in Fig. 2 for $F = 1.5 F_{th}$. The white circle surrounds the area of the crater that will be left by the front pulse. Only the energy included

in that circle will effectively contribute to the ablation. **B**—3D visualization of the additional free interface for same overlaps of A. The violet volume is the affected by the portion of energy deposited in A. The boundary in light blue represents the new free interface where the material is no longer constrained

by the spatial intensity profile over that area. Figure 6a shows for illustration purposes only the effective intensity profile incident on the thin film surface for different overlaps. For pulse overlap $O = 2$, the incident energy calculated by integrating the laser intensity profile on the freshly exposed target area drops by 50% with respect to the single pulse case; for $O = 4$ this energy is 22% and for $O = 8$ only 10%. Furthermore, for all laser pulse overlap values above 1 $O > 1$ this freshly irradiated volume from the second and subsequent arriving pulses is not completely confined because the previous pulse has partially released the edges of the irradiated spot along the scanning direction (Fig. 6b). In this case, the material can freely expand on one side which is different to the very first pulse exposing a virgin surface. Since the material is no more spatially constrained the radial reaction forces generated during the rapid expansion of the material after the pulse (i) will be reduced in amplitude and (ii) will not add to provide a net component pointing normally away from the substrate as described in the previous paragraphs. The presence of the free boundary also decreases the amount of potential energy stored in the metal layer because the film temperature rise cannot be followed by a strongly coupled rarefaction and subsequent pressure rise locally as in the fully confined case. This is why the first pulse of each channel always ablate: independently from the overlap the first pulse will always hit virgin material. Therefore, the beginning of each line will experience the

single pulse case where temperature and pressure rises are fully confined. Finally, the closer the fluence is to the ablation threshold value, the lower is the available energy in excess of E_{ten} for fracturing the film. It also means that, the closer is the process to F_{th} , the smaller is the conversion efficiency loss that can be sustained by the system before dropping the rarefaction wave energy below E_{ten} . As a result, approaching F_{th} , ablation termination will start at lower overlap.

It has been discussed why $E_{ad} \ll E_{ten}$ for a single pulse ablation case. By increasing the pulse overlap, the removal process can be so inefficient that the stored potential energy is close to the adhesion energy, giving $U \approx E_{ad}$. For such an overlap range, the energy coupled into tensile stress can be high enough to delaminate the film irradiated area but not enough to fully rupture it. This is especially true when the pulse to pulse distance is so small that only the low energy outer wings of the incident Gaussian beam irradiate any fresh material. In this case, the front end of each laser pulse along the scanning direction, will progress further the layer delamination front by the inter-pulse firing distance (Fig. 7). On the opposite side, the central and trailing regions of the pulse are incident on an area completely detached from the substrate, where the metal layer can almost freely expand along the vertical direction. Without the mechanical confinement imposed by the substrate, the net force along the thickness of the free standing film is zero, and hence the material does not move.

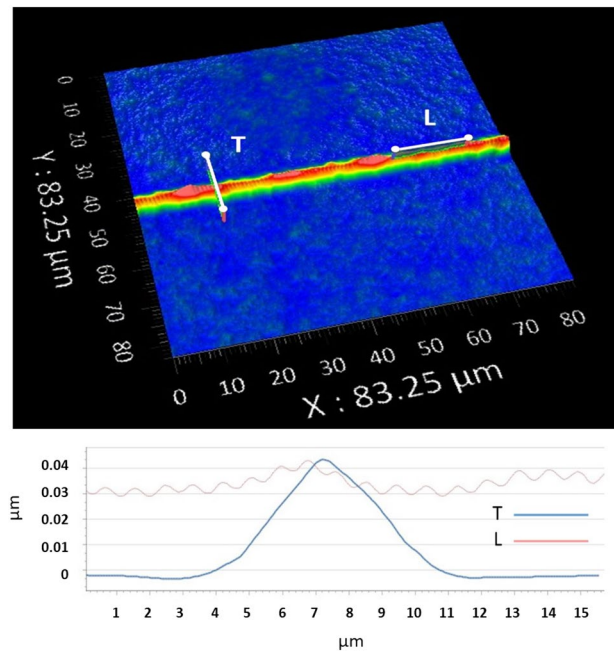


Fig. 7 Longitudinal and transversal sections of the case $O=8.5$ presented in Fig. 2. We can see that the line is delaminated and the material is not removed. The longitudinal section shows that the delamination is modulated with periodicity equal to the inter-pulse distance

The thermal conductivity of gold is 318 W/m K, that of a generic polymer is 0.2 W/m K while for air is 0.02 W/m K. For the irradiated disk of thickness d and base area A , the ratio between the area of its surrounding wall and the its base is 23. Since the difference between the gold thermal conductivity and the other materials at its interface is more than three (3) orders of magnitude, we can assume that the main heat flux during the ablation process is through the side walls of the irradiated volume, whilst any heat flowing through the remaining interfaces is negligible. This also suggests that the impact of film lift-off on the heat dissipation is small, because losing the contact with the substrate will not significantly change much the film heat dissipation. For the single pulse case the main source of cooling is probably material removal: most of the heat is carried away from the substrate with the ablated flyer. However, once the overlap needed for ablation termination is reached the material remains on the surface. Without any cooling by material removal the surface film temperature rises quickly by cumulative pulse exposure with increasing overlap. Eventually, a certain overlap is reached when heat dissipation through the side walls of the irradiated disk is insufficient to maintain the temperature below the melting point. Once the gold layer melting temperature is reached ablation starts again triggered presumably by cumulative pulse exposure thermal effects.

4 Conclusion

The effectiveness of the laser spallation process relies on the thermoelastic stress forces generated within the irradiated volume in thin film ablation. If less laser energy is absorbed within the irradiated volume, or the thermoelastic stresses are easily dissipated, the effectiveness of the spallation process can be reduced by a few orders of magnitude. By increasing the spatial laser pulse overlap, it is, therefore, possible to weaken such thermoelastic stress and therefore change the removal process mechanism. Above ablation threshold and for low pulse overlap, the well-known single pulse spallation mechanism applies. By increasing the pulse overlap over a certain value, at fluences close enough to the ablation threshold, material removal can be terminated. In such regime, thermoelastic stress can only lift-off the film irradiated area despite the fluence being above the single pulse ablation threshold. Along the line scanning direction, the front end of the pulse grows film delamination, while the core of the intensity profile intercepts a detached metal region from the substrate. As long as the pulse overlap does not increase to the point, where the free standing delaminated material cannot dissipate anymore the cumulative deposited heat, this regime remains unaltered. Once the overlap is so high that the layer melting point is reached, thermal ablation overtakes mechanical spallation permanently as the main removal process. Future work will focus on the control of this effect for industrial applications by reshaping the intensity profile from Gaussian to top-hat, studying the effects of the repetition rate at constant overlap and analyzing its material dependency.

Acknowledgements Riccardo Geremia is an engineering doctorate student at the EPSRC Centre for Doctoral Training in Applied Photonics (EP/L01596X/1), based at Heriot Watt University. Riccardo Geremia wishes to thank Oxford Lasers Ltd. for sponsoring the engineering doctorate. This work is partially funded by the European project HIPER-LAM, grant agreement 723879. We also would like to thank FlexEnable Ltd. for providing the thin film samples under study.

Open Access This article is distributed under the terms of the Creative Commons Attribution 4.0 International License (<http://creativecommons.org/licenses/by/4.0/>), which permits unrestricted use, distribution, and reproduction in any medium, provided you give appropriate credit to the original author(s) and the source, provide a link to the Creative Commons license, and indicate if changes were made.

References

1. X. Liu, D. Du, G. Mourou, IEE J. Quant. Electron. **33**(10), 1706 (1997)

2. C. Momma, B.N. Chichkov, S. Nolte, F. von Alvensleben, A. Tünnermann, H. Welling, B. Wellegehausen, *Opt. Commun.* **129**, 134 (1996)
3. G. Paltauf, P.E. Dyer, *Chem. Rev.* **103**, 487 (2003)
4. R.S. Dingus, R.J. Scammon, *SPIE Proc.* **1427**, 45 (1991)
5. P. Lorenz, M. Ehrhardt, L. Bayer, K. Zimmer, *Phys. Procedia* **83**, 240 (2016)
6. P.-O. Westin, U. Zimmermann, M. Ruth, M. Edoff, *Sol. Energy Mater. Sol. Cells* **95**, 1062 (2011)
7. D. Karnakis, A. Kearsley, M. Knowles, *J. Laser Micro. Nanoen.* **4**(3), 218 (2009)
8. N. Bellini, R. Geremia, S. Norval, G. Fichet, D. Karnakis, *J. Laser Micro/Nanoeng.* **11**, 388 (2016)
9. N. Bellini, R. Geremia, D. Karnakis, *Appl. Phys. A* **123**, 347 (2017)
10. J.L. Liu, *Opt. Lett.* **7**(5), 196 (1981)
11. S.G. Koulikov, *J. Photochem. Photobio. A* **145**, 183, (2001)
12. D.D. Dlott, *Appl. Surf. Sci.* **197**, 3 (2002)
13. Y.B. Zel'dovich, *Physics of shock waves and high temperature hydrodynamics phenomena* (Dover publications, New York, 2002)
14. P.K. Sharma, N. Singh, *Phys. Rev.* **1**, 4635, (1970)
15. S. Timoshenko, *Theory of Plates and Shells* (McGraw-Hill, New York, 1959)
16. H.D. Espinosa, B.C. Prorok, M. Fischer, *J. Mech. Phys. Solids* **51**, 47 (2003)
17. A. Catlin, W.P. Walker, *J. Appl. Phys.* **31**, 2135 (1960)
18. B.C. Stuart, *Opt. Soc. Am. B* **13**(2), 459 (1996)
19. J. Kruger, *Appl. Surf. Sci.* **253**, 7815 (2007)
20. R.D. Emery, G.L. Povirk, *Acta Materialia*. **51**, 2067, (2003)